Chirality Effects on Peptide Self-Assembly Unraveled from Molecules to Materials

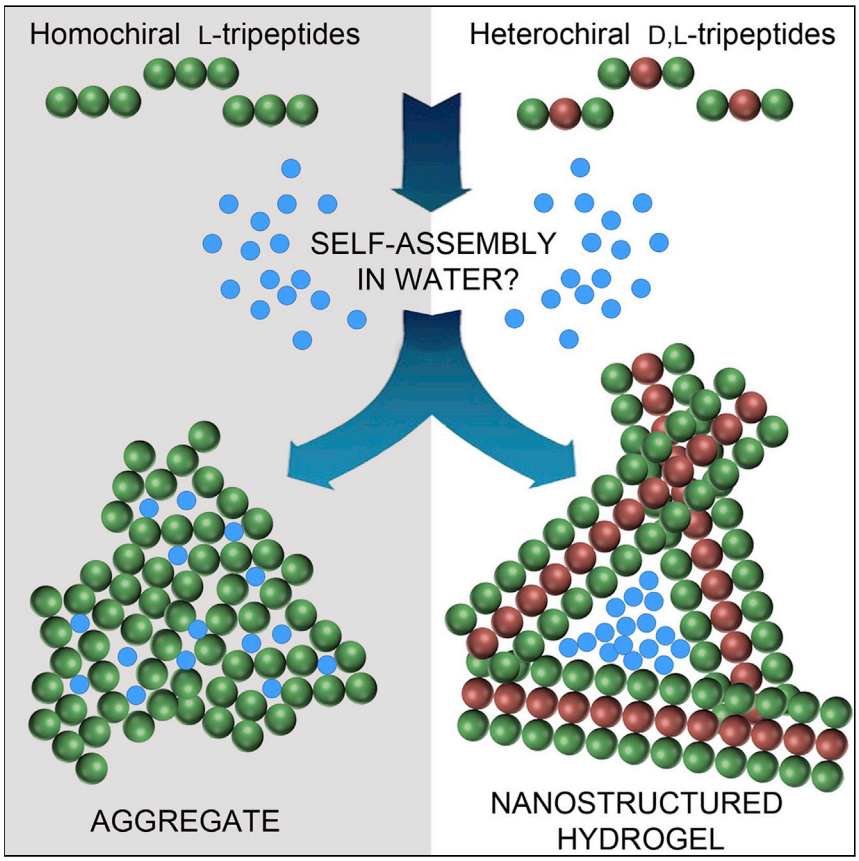

This work explains why and how heterochiral and homochiral tripeptides differ in their assembly in water. A characteristic spectroscopic signature is assigned to molecular conformation. We monitor the process as a continuum from the molecular scale to the macroscopic biomaterials so that the final properties are linked to chemical structure of the building blocks. This work lays the foundation for the design of supramolecular hydrogel biomaterials based on short sequences of hydrophobic D- and L-amino acids.

Ana M. Garcia, Daniel Iglesias, Evelina Parisi, ..., Michele Melchionna, Attilio V. Vargiu, Silvia Marchesan

vargiu@dsf.unica.it (A.V.V.)
smarchesan@units.it (S.M.)

HIGHLIGHTS

We explain how and why homochiral and heterochiral peptides differ in hydrogelation

Spectroscopic signature is assigned to characteristic molecular conformation

Self-assembly is monitored continuously from the angstrom to the macroscopic scale

Design rules that link (bio)material properties to chemical structure are provided

Chirality Effects on Peptide Self-Assembly Unraveled from Molecules to Materials

Ana M. Garcia,[1] Daniel Iglesias,[1] Evelina Parisi,[1] Katie E. Styan,[2] Lynne J. Waddington,[2] Caterina Deganutti,[1] Rita De Zorzi,[1] Mario Grassi,[3] Michele Melchionna,[1] Attilio V. Vargiu,[4,*] and Silvia Marchesan[1,5,*]

SUMMARY

Self-assembling short peptides are attractive minimal systems for mimicking the constituents of living systems and building (bio)materials. The combination of both D- and L-amino acids into heterochiral sequences is a versatile strategy for building durable supramolecular architectures, especially when their homochiral analogs do not self-assemble. The reasons for this divergent behavior have remained obscure until now. Here, we elucidate how and why homochiral and heterochiral peptides behave differently. We identify a key spectroscopy signature and its corresponding molecular conformation, whereby an amphiphilic structure is uniquely enabled by the peptide stereochemistry. Importantly, we unravel the self-assembly process as a continuum from the conformation of single molecules to their organization into nano- and microstructures and through to macroscopic hydrogels, which are probed for cytotoxicity in fibroblast cell culture. In this way, (bio)material properties at the macro-scale can be linked to the chemical structure of their building blocks at the angstrom scale.

INTRODUCTION

Peptides self-assemble to make up the materials of life. The fine-grained details of their organization give rise to useful properties, from the toughness of spider silk to the delicate dynamism of the structures of the cytoskeleton. Knowledge of how peptide self-assembly works in minimal systems—those comprising only a few amino acid residues—could provide a basis for understanding how more complex protein assemblies form, and it is also expected to allow the generation of useful materials. The functional materials formed by self-organizing minimalist peptides have high value.[1] Their applications include drug delivery,[2] tissue engineering,[3] biomimicry,[4] cancer cell detection,[5] and even vaccine adjuvants to stimulate the immune response[6] through to uses as emulsifiers,[7] pigments,[8] catalysts,[9] and semiconductors.[10] Peptides stand out for their chemical diversity, low impact on the environment, and ability to convey biological messages in sequences as short as three amino acids.[11] However, it is less well understood that non-proteogenic D-amino acids play crucial roles in short bioactive motifs, such as D-Phe in fibronectin mimics for integrin engagement[12] and D-Ala in dermorphin for opioid receptor binding.[13] D-amino acids are also attracting attention for their emerging role in brain neurotransmission.[14,15] In addition, they are known to bestow resistance against enzymatic hydrolysis and stability upon specific peptide conformations, such as β turns.[16] Such findings generate motivation for employing D-amino acids in simple building blocks for supramolecular biomaterials, where structure and function are entwined.

The Bigger Picture

Nature makes pervasive use of homochirality (e.g., D-sugars and L-peptides) to assemble biomolecules, whose interactions determine life processes. D-amino acids rarely occur, and their effects are not yet completely understood. For a long time, structural complexity (e.g., polypeptides and constrained molecules) was considered a requirement for achieving defined conformations that ultimately allow biomolecule recognition and function.

Here, we detail how minimalist building blocks can adopt conformations with a characteristic spectroscopic signature, whereby substitution of just one L-amino acid for its D mirror image leads to a divergent path for assembly in water. Subtle molecular variations are amplified through increasing size scale all the way to macroscopic differences that are visible to the eye. Ultimately, the design of heterochiral (bio) molecules thus provides an alternative approach to shed new light on the supramolecular interactions that define life as we know it.

In light of the cost of large-scale peptide production, the search is very active for the smallest motifs capable of achieving a chosen function. Hydrogel formation is a useful feature that is, unfortunately, difficult to predict. Computational approaches are proving useful in the search for gel-forming peptides, especially for derivatives bearing rigid aromatic groups that dominate self-assembly behavior, such as fluorenyl (in Fmoc) or naphthalene.[17] However, concerns exist over the fate of these modified peptides *in vivo* and thus over their biological application.[18,19] Successful prediction of gel formation is most difficult for the shortest unprotected peptides. For example, only four gelators were experimentally identified by an *in silico* analysis of all 8,000 combinations of L-amino acids in trimers.[20] There is thus large scope for new approaches to the discovery[21] or the rational design of short peptides able to gel, especially under physiological conditions. Advances in this area could provide innovative means of therapy by eliciting a biological response through assembly *in vivo*.[22] In addition, the combination of both L- and D-amino acids in short peptides could provide a unique approach to fine-tuning their lifetime in biological settings and to shedding light on nature's pervasive choice for homochirality. Ultimately, understanding the effects of D-amino acids in short-peptide self-organization could advance therapeutic solutions for amyloidoses,[23] implicated from neurodegeneration[24] to diabetes,[25] as well as for infections linked to biofilm formation.[26]

The design of peptides that self-assemble to form hydrogels requires a fine balance between hydrophobic and hydrophilic content so as to achieve aggregation while allowing favorable interactions with water to avoid precipitation. Such amphiphilic structures are typically obtained by intra-peptide segregation of hydrophilic and hydrophobic amino acids, i.e., in α helices, which require longer peptides composed of heptad repeats.[27] Alternatively, amphiphilic β sheets are formed by the alternation of ionic and hydrophobic amino acids (Figure 1A).[28] The inclusion of hydrophilic amino acids in unprotected L-tripeptides has been an essential feature in obtaining amphiphilic assemblies that gel.[20,29]

Here, we detail a concept of hydrogel formation by using the peptide backbone as the only hydrophilic component. We infer the alternation of D- and L-amino acids to favor an amphiphilic β conformation that is effective for self-assembly and gelation in a peptide of only three residues. Our approach leads hydrophobic side chains and hydrophilic backbone groups to be displayed on opposite sides of the peptide (Figure 1B). The effects of heterochirality upon unprotected (tri)peptide gelation have been observed in isolated examples,[30–33] but a conceptual framework for understanding these effects has been lacking until now. Our study aims to provide such a framework by unveiling the effects of fine structural changes on peptide conformation and consequent packing into soft materials and thus on their macroscopic properties. The rational design of a series of hydrogelators (Figure 1C and Table 1) was accompanied by both *in silico* and experimental investigations of self-assembly from the initial monomer state through each stage and length upscaling to the macroscopic material, which was then probed for cytotoxicity via cell culture. Importantly, we have identified a key circular dichroism (CD) signature and its correspondence with peptide conformation, revealing how homochiral and heterochiral analogs are similar and differ in the domino process leading to macroscopic gelation.

RESULTS AND DISCUSSION

Rational Design of Self-Assembling Tripeptides

A series of hydrophobic ^{L}Phe-^{D}Xaa-^{L}Phe tripeptides, where ^{D}Xaa is an aliphatic D-amino acid (Figure 1C and Table 1), was prepared by solid-phase peptide

[1]Department of Chemical & Pharmaceutical Sciences, University of Trieste, 34127 Trieste, Italy

[2]CSIRO Manufacturing, Clayton, VIC 3168, Australia

[3]Department of Engineering and Architecture, University of Trieste, 34127 Trieste, Italy

[4]Department of Physics, University of Cagliari, 09042 Monserrato, Italy

[5]Lead Contact

*Correspondence: vargiu@dsf.unica.it (A.V.V.), smarchesan@units.it (S.M.)

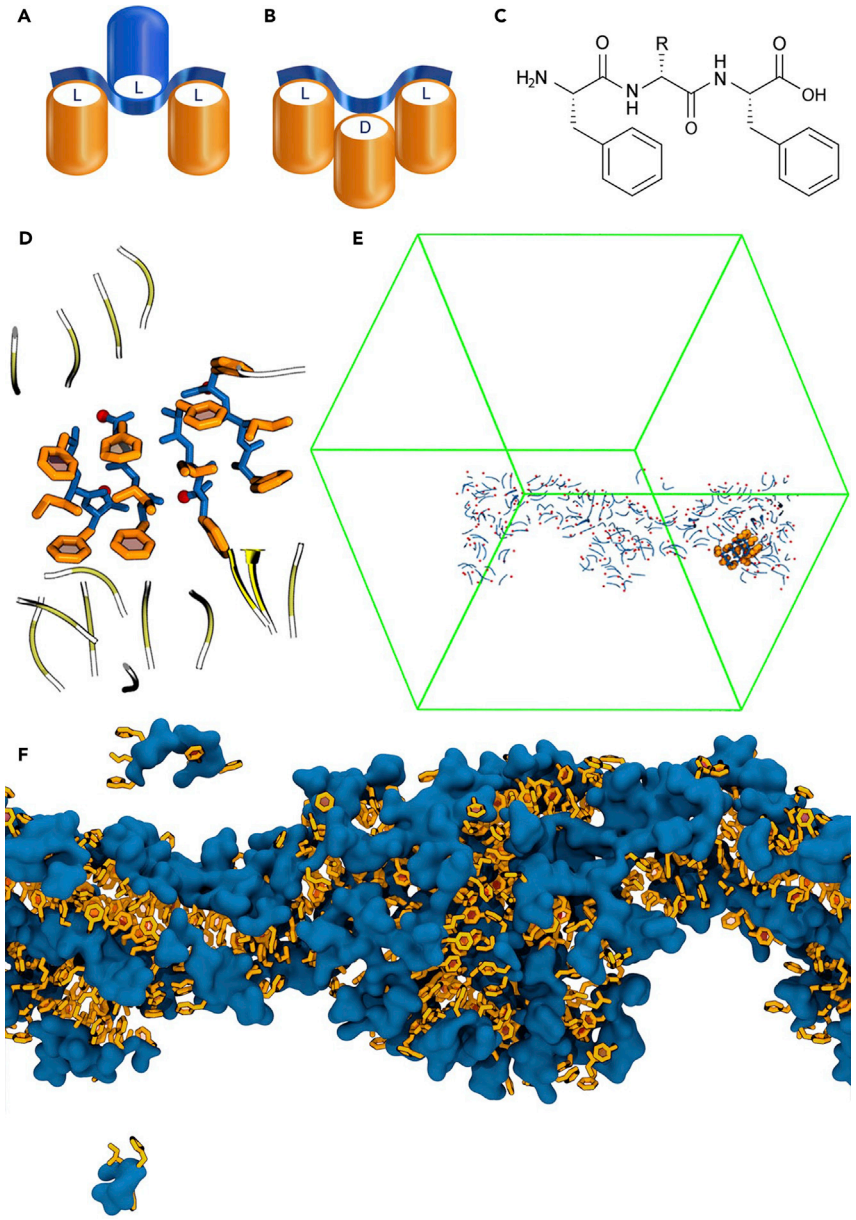

Figure 1. Tripeptides Containing Alternating L- and D-Amino Acid Residues Generate Amphipathic Fibers

(A and B) Traditional design alternates hydrophilic (blue) and hydrophobic (orange) L-amino acids to create amphipathic structures (A), whereas in this study, the alternation of L- and D-hydrophobic amino acids generates amphiphiles where the hydrophilic component is the peptide backbone (blue string) (B).

(C) A generic tripeptide sequence structure (see Table 1 for a list of R side chains).

(D–F) MD simulations of Phe-^{D}Ile-Phe in explicit water show amphiphilic β sheets interdigitating into fibers within nanoseconds, wherein peptide stacks (D) display hydrophobic side chains on the same side of the peptide backbone; these side chains are highlighted in orange in the MD box (E) containing 216 peptides that self-organize into amphipathic nanofibrils (F; peptide oxygen and nitrogen atoms and water oxygen atoms within 2 Å from peptides are shown as a blue surface).

synthesis and purified by high-performance liquid chromatography (HPLC). This series included all naturally occurring side-chain lengths (i.e., methyl, propyl, and butyl groups) and all possible branching options (i.e., β-branched, γ-branched, or linear

Table 1. Phe-^{D}Xaa-Phe Peptides of This Study

^{D}Xaa	R	LogP	HPLC Retention Time (min)	MGC (mM)
Alanine (Ala)	$-CH_3$	1.50 ± 0.20	7.3	NA
Valine (Val)	$-CH(CH_3)_2$	2.39 ± 0.21	8.0	9.5
Norvaline (Nva)	$-CH_2CH_2CH_3$	2.47 ± 0.32	8.0	9.5
Isoleucine (Ile)	$-CH(CH_3)CH_2CH_3$	2.83 ± 0.27	8.3	8.0
Leucine (Leu)	$-CH_2CH(CH_3)_2$	2.76 ± 0.32	8.4	5.0
Norleucine (Nle)	$-CH_2CH_2CH_2CH_3$	2.91 ± 0.38	8.4	5.0

The series includes different central amino acids (^{D}Xaa) with aliphatic side chains (R); hydrophobicity (based on logP[34] and experimental HPLC retention time) correlates with minimum gelling concentration (MGC). NA, not available.

side chain) for common building blocks to allow a thorough correlation between chemical structure and assembly. The alternation of D and L handedness was designed to yield two-faced amphiphilic supramolecular β sheets, as predicted by molecular dynamics (MD) simulations in explicit water.[35] Superstructures were designed to be held together by an ordered pattern of hydrogen bonding between amides and by salt bridges between the charged ammonium and carboxylate termini, which together provide the hydrophilic content (see Figure S41). The presence of Phe at both termini allowed interdigitation between stacks into supramolecular zippers that exclude water.[32] Indeed, MD showed that within nanoseconds, Phe-^{D}Ile-Phe formed stacks that converged into elongated fibers approximately 5 nm in diameter (Figures 1D–1F and Video S1).

CD Signature and Peptide Conformation in Solution

In the monomer state, this series of heterochiral tripeptides displayed a characteristic CD signature (Figures 2A and S42) that was very different from that of more commonly observed conformations (e.g., α helix, β sheets, and random coils). The molar ellipticity did not change after sample dilution at different concentrations that were well below the minimum gelation concentration (MGC), confirming a monomeric state.

The naturally occurring L-tripeptides Phe-Xaa-Phe (Xaa = Ala, Val, Nva, Leu, Ile, or Nle) served as controls, leading us to infer this CD signature to be a result of predominant L configuration (Figures 2A and S42), as reported for self-assembling Phe-Glu-Phe in solution[36] as well as for non-assembling L-peptides containing Phe.[37] However, the physical origin of this CD signature in terms of peptide conformation(s) remains obscure. We hypothesize that it is due to a statistical coil, whereby unfolded peptides sample specific conformational states that co-exist in equilibrium. The two positive maxima observed at 199 and 219 nm are assigned to $\pi \rightarrow \pi^*$ and $n \rightarrow \pi^*$ transitions of the peptide bonds, respectively, and their CD signatures are thus affected by the relative orientations of the corresponding dipoles of the two amides, as well as interactions with their environment.

Comparison of the conformations of self-assembling Phe-^{D}Ile-Phe and Phe-^{D}Leu-Phe and the non-gelling L-peptide Phe-Ala-Phe helps to elucidate how self-assembly works in heterochiral tripeptides (Figures 2B–2E). Phe-^{D}Ile-Phe and Phe-^{D}Leu-Phe are the most sterically hindered amino acids that are branched at the β and γ positions, respectively. L-Phe-Ala-Phe is homochiral and displays the least steric hindrance. In the monomeric state, the self-assembling tripeptides sample three principal conformations (accounting for ca. 90% of the population; see Figure S43),

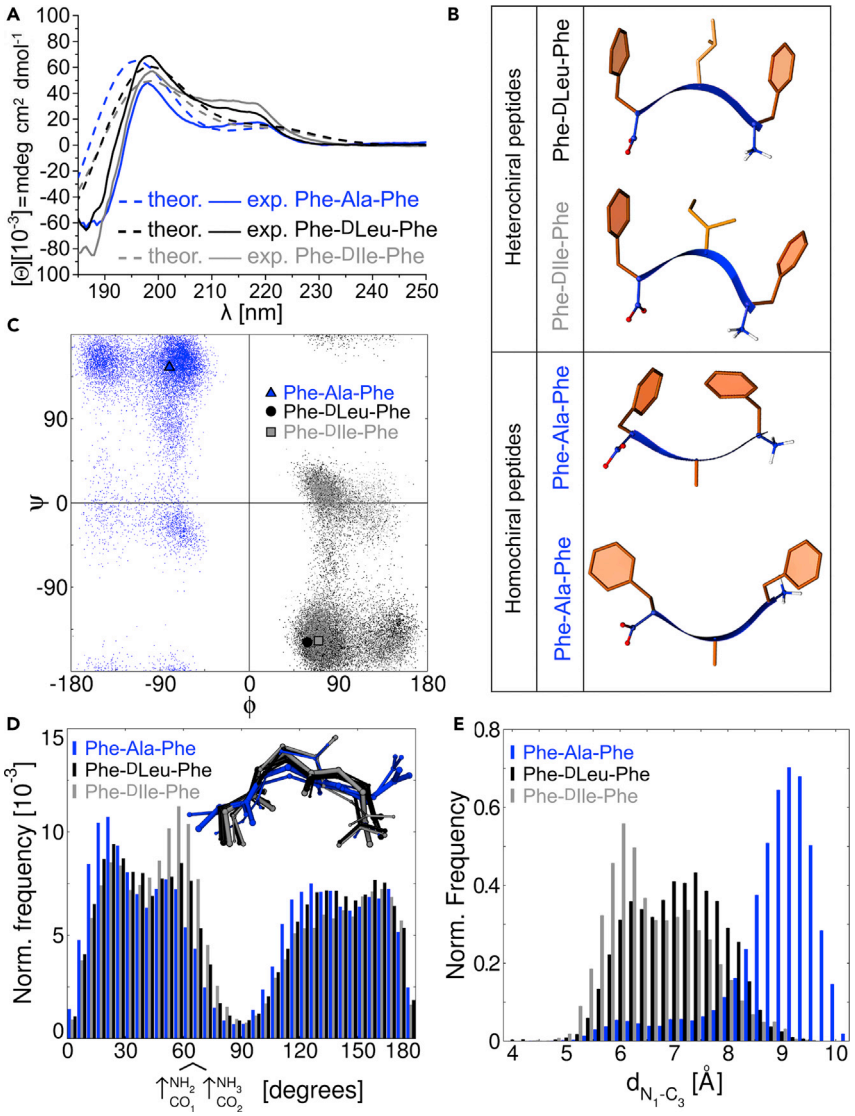

Figure 2. Why Heterochiral Peptides Self-Assemble but Their Homochiral Analogs Do Not

(A) Calculated and experimental circular dichroism (CD) spectra for three representative tripeptides.

(B) Favored amphiphilic conformation (hydrophobic side chain in orange and hydrophilic backbone in blue) for self-assembling tripeptides and the two equally most stable conformations for Phe-Ala-Phe.

(C) Ramachandran plot highlighting the most frequent conformations for the three tripeptides studied.

(D) The relative dipole orientation distributions are analogous for the three tripeptides studied, as confirmed by the superimposable peptide backbones of the three most stable conformations of the three peptides.

(E) N-to-C distances confirm the L-tripeptides to have more extended structures than the heterochiral tripeptides.

of which the most representative is displayed in Figure 2B. Although the side-chain branching differences between Ile and Leu are known to favor different conformations,[38,39] here there is a striking similarity between the two: both adopt an amphiphilic conformation. Their aliphatic side chains are sandwiched between the two Phe aromatic rings, creating a hydrophobic region that effectively excludes water and

leads the backbone to turn, whereas the charged termini are displayed on the opposite side of the peptide backbone, as design dictates.

Phe-Ala-Phe, being the least sterically hindered tripeptide, displayed more freedom and sampled two dominant conformations nearly equally (Figure 2B). Also in this case, the Phe side chains were on the opposite side of the peptide backbone from the charged termini, but the L-Ala hydrophobic methyl side chain was projected into the otherwise hydrophilic region, leaving a void between the aromatic rings. As a result, Phe-Ala-Phe did not display an overall amphiphilic conformation with net segregation of aliphatic side chains and hydrophilic components.

Peptide and protein structures are described with Ramachandran plots, whereby specific combinations of backbone dihedral angles Φ and Ψ correspond to defined conformations (e.g., β sheets, α helices, etc.).[40] Ramachandran plots of the three model peptides (Figure 2C) showed a common trend, considering that D-peptide regions are analogous to L-peptides when inverted through the center of the plot. The dihedral angles for the predominant conformations are overlaid in the Ramachandran plot. All are located in a β-strand area, and the second residue has Φ and Ψ angle combinations that are found in type II β turns (i.e., $[-60°, +120°] \pm 30°$).[41] Although these unprotected tripeptides are too short to fulfill all of the requirements for the canonical definition of a turn,[42] these conformations can be considered turns on the basis of the overall change of direction of the peptide backbone and of the <7 Å $C_{\alpha 1}$-$C_{\alpha 3}$ distance (see Table S3).[41] Importantly, the peptide backbones of the three most frequently observed conformations for each tripeptide are nearly superimposable (inset in Figure 2D). Indeed, the relative dipole orientations of the peptide bonds reveal analogous distributions (Figure 2D), in agreement with their similar CD signatures. Correspondence between CD spectra and conformations is supported by theoretical CD spectra calculated for the MD conformations (dashed traces in Figure 2A), which show the same trends observed in the experimental data (continuous lines in Figures 2A and S42).

However, only heterochiral L-D-L tripeptides displayed the three hydrophobic side chains on the same side of the peptide backbone, where their mutual interactions favored a turn overall by excluding water molecules (Figure 2B). In contrast, L-tripeptides did not experience such an effect, and their backbones stayed more extended, as supported by MD-calculated N-to-C distances, which were shorter for self-assembling tripeptides (Figure 2E).

Single-Crystal XRD Structures

Single-crystal X-ray diffraction (XRD) data revealed a dramatic difference between the packing of heterochiral and homochiral tripeptides (Figure 3 and Table S1). Phe-^{D}Nva-Phe displayed an amphipathic conformation with net segregation of hydrophobic and hydrophilic components on opposite sides of the backbone, as predicted by MD studies. The latter faced the interior of 2.0-nm-wide water channels, whereas the former created hydrophobic regions whereby amino acid side chains from different channels interdigitated and held the structure together (Figures 3A and S1). By contrast, single-crystal XRD data for Phe-Ala-Phe revealed an extended conformation incapable of fully separating hydrophilic (blue) and hydrophobic (orange) components, given that the hydrophobic Ala side chain impinged upon the hydrophilic region containing water molecules. As a net result, water channels were not formed by the homochiral tripeptide (Figures 3B and S2).

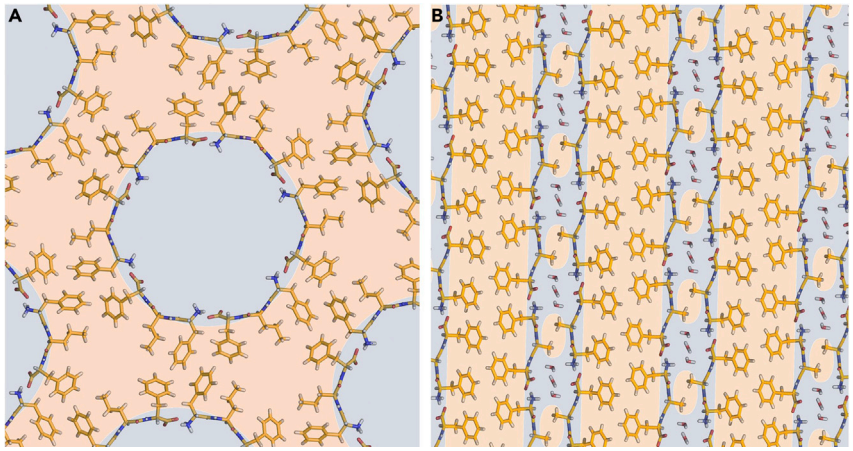

Figure 3. Single-Crystal XRD Data Reveal Very Different Packing for Heterochiral and Homochiral Peptides

(A) Phe-^{D}Nva-Phe packing shows net segregation of hydrophobic (orange) and hydrophilic (blue) components, allowing the formation of 2.0-nm-wide water channels.

(B) Homochiral Phe-Ala-Phe packs into layers, whereby the Ala methyl side chain impinges in an otherwise hydrophilic region.

This combination of crystallographic, MD, and spectroscopic evidence thus provides a clear picture of why heterochiral peptides self-assemble to form hydrogels but their homochiral analogs do not. In light of these findings, we infer that a similar mechanism could drive the formation of nanostructured hydrogels by other tripeptides featuring scrambled sequences of D- and L-hydrophobic residues with only one Phe at the termini (e.g., Val-^{D}Phe-Phe,[30] ^{D}Val-Phe-Phe,[30] ^{D}Phe-Phe-Val,[31] ^{D}Leu-Phe-Phe,[32] ^{D}Phe-Phe-Ile,[33] His-^{D}Phe-^{D}Phe,[43] etc.). Similarly, amphipathic conformations, as well as the formation of dry steric zippers that exclude water and hold the superstructures together, are expected. However, differences between building blocks are likely to result in packing variations, whereby water channels, when formed, can vary in diameter and overall topology. Expansion of design rules to a more diverse toolbox of heterochiral peptides thus opens the way to exciting possibilities for the design of supramolecular channels and functional architectures.

Monitoring Peptide Conformation during Assembly and Disassembly

Tripeptides were first added to alkaline phosphate buffer, where they dissolved as a result of electrostatic repulsion between their negative charges. Neutralization of the pH was then used for probing self-assembly and hydrogelation of the resulting zwitterions, which are capable of engaging in salt bridges given a favorable peptide conformation. Molar ellipticity of CD spectra did not change significantly for non-gelling Phe-Xaa-Phe (Xaa = Ala, Val, Nva, Leu, Ile, or Nle) L-analogs and Phe-^{D}Ala-Phe relative to their monomeric state in dilute samples (see Figure S44). For all of the other self-assembling D,L-tripeptides, assembly over time and disassembly upon heating were monitored by CD (see Figures 4 and S46), confirming visual observations (see Table S4). All peptide hydrogels showed thermoreversibility, although gel-to-sol transitions occurred at different temperatures, reflecting the increasing stability of their supramolecular structures as hydrophobicity increased.

CD signature was qualitatively preserved across most gel-forming peptides, suggesting that peptide conformation did not change significantly from the monomeric state, in agreement with MD data (compare Figure 1D with Figure 2B). By contrast,

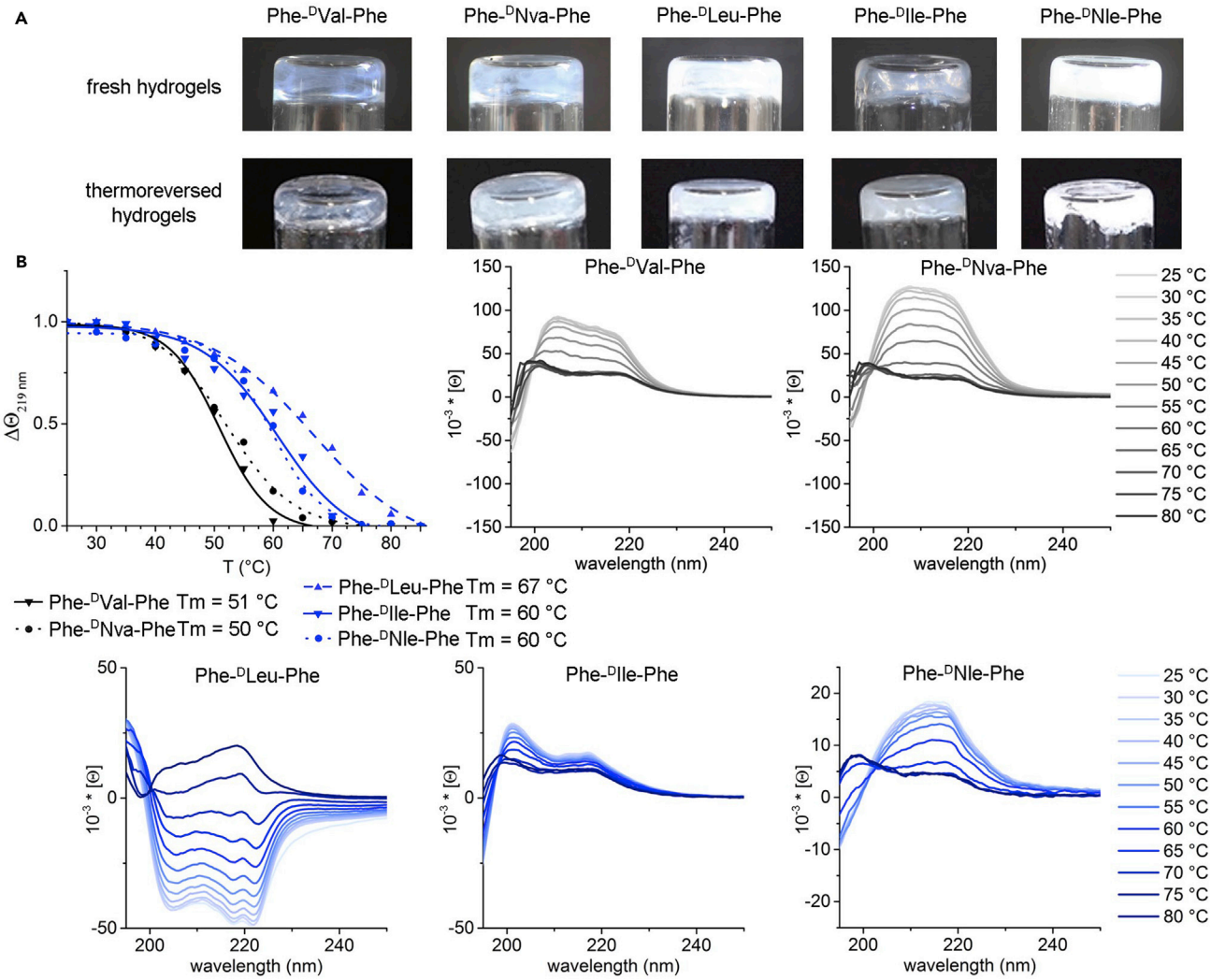

Figure 4. Peptides Form Thermoreversible Hydrogels

(A) Photographs of fresh (top) and thermoreversed (heated then cooled; bottom) tripeptide hydrogels.

(B) Monitoring of supramolecular structure by CD over a temperature ramp up to 80°C. Melting temperature (Tm) can be determined by plotting molar ellipticity [Θ] at 219 nm as the temperature is increased. Data for peptides bearing valine isomers are depicted in gray, and those for leucine isomers are depicted in blue.

quantitative differences were ascribed to variations in peptide spatial arrangement upon stacking into supramolecular structures, which ultimately led to hypochromic and hyperchromic shifts. The majority of peptides displayed a broad, positive CD signal in the region of 200–220 nm, which is compatible with β structures of D-chirality, as previously observed for other L-D-L self-assembling tripeptides.[30,31] Phe-^{D}Leu-Phe was the only peptide exhibiting a negative CD signal in the assembled state, yet MD analysis did not reveal significant differences relative to Phe-^{D}Ile-Phe other than an increased twist in the pleated β sheets, which were significantly more planar in the latter case (see Figure S47). These data suggest that differences in CD spectra can be ascribed mainly to higher-order organization of the fibrils rather than different peptide conformations. Attenuated total reflectance infrared spectroscopy data supported this hypothesis; one predominant amide I signal was centered at 1,645–1,651 cm^{-1} for all peptides (see Figure S48). This signal is close to the expected β-sheet signal, as was observed for other self-assembling L-tripeptides.[20]

The narrowest amide I signal was displayed by Phe-^{D}Leu-Phe, followed by the other gelators, providing an indication of homogeneous conformation and high degree of supramolecular order. By contrast, the broadest amide I signal with multiple maxima was displayed by non-assembling peptide Phe-^{D}Ala-Phe, indicating sample heterogeneity and the presence of different conformations.

Self-Assembled Nanostructure Morphology and Rheological Properties

Peptide Phe-^{D}Ala-Phe was the least hydrophobic and sterically hindered of the series, and no hydrogel or ordered nanostructure was observed to form as expected (see Figures S45, S56, and S57). By contrast, all other heterochiral samples formed nanostructured hydrogels, as revealed by atomic force microscopy (AFM), transmission electron microscopy (TEM), cryogenic TEM (cryo-TEM) imaging, and rheometric analyses (Figures 5 and S58–S68). Samples composed of thinner fibrils were more transparent, whereas those containing thicker bundles appeared opaque white. No hydrogel was obtained from homochiral analogs, even when their concentration exceeded their solubility limit (Figures S45 and S69).

With regard to nanomorphology, TEM and AFM revealed that the majority of homochiral controls formed amorphous aggregates (Figures S49–S55); however, Phe-Ala-Phe showed a tendency toward the formation of microcrystals, thus allowing us to investigate its structure by single-crystal XRD (see above). By contrast, heterochiral peptides, both displaying Val or Leu isomers, all assembled into fibrils but were diverse in terms of rigidity and tendency toward branching or bundling (Figure 5A). In particular, the presence of amino acids with side-chain branching closer to the peptide backbone (i.e., at the β-position for ^{D}Val and ^{D}Ile) promoted branching as opposed to bundling. The net result was that peptides bearing ^{D}Val and ^{D}Ile formed thinner fibrils of narrower diameter distribution that were better interconnected in hydrogel networks. Phe-^{D}Val-Phe and Phe-^{D}Ile-Phe formed flexible fibrils as thin as 7 $\pm$ 2 and 8 $\pm$ 2 nm (n = 100), respectively, that occasionally wound up in numbers of two to three (average diameter = 15 $\pm$ 4 and 15 $\pm$ 5 nm [n = 25], respectively). Instead, Phe-^{D}Leu-Phe assembled into 11 $\pm$ 2-nm-wide (n = 100) fibrils, which for the majority ran parallel to each other or bundled in stiffer fibers very diverse in thickness, i.e., 47 $\pm$ 37 nm (n = 100). Phe-^{D}Nva-Phe assembled into 16 $\pm$ 3-nm-wide fibrils, which for the majority entangled into bundles of heterogeneous dimensions (average diameter = 76 $\pm$ 27 nm [n = 50]). The presence of amino acids with linear side chains (i.e., ^{D}Nva or ^{D}Nle) allowed peptides to pack efficiently into hierarchical structures, resulting in stiffer and thicker fibers and, in the extreme case of ^{D}Nle, straight, nearly micron-thick, bundles.

In terms of rheological properties (Figure 5B), the stability of heterochiral peptide supramolecular structures appeared to increase with steric hindrance, such that peptides containing four methylene units (i.e., ^{D}Ile, ^{D}Leu, or ^{D}Nle) surpassed in stability those containing only three (i.e., ^{D}Val or ^{D}Nva). The former had faster gelation kinetics and higher elastic moduli G′. Interestingly, the presence of amino acids with linear side chains (i.e., ^{D}Nva or ^{D}Nle), which promoted hierarchical assembly and bundling into thick and rigid fibers as discussed above, negatively affected hydrogel resistance against applied stress, as exemplified by the ^{D}Nle peptide, which was observed to segregate from the aqueous phase. On the contrary, the presence of amino acids with β branching (i.e., ^{D}Val or ^{D}Ile), which promoted the formation of a dense network with a higher level of interconnectivity between flexible and thin fibrils, led to hydrogels that exhibited more resistance against applied stress than their structural isomers.

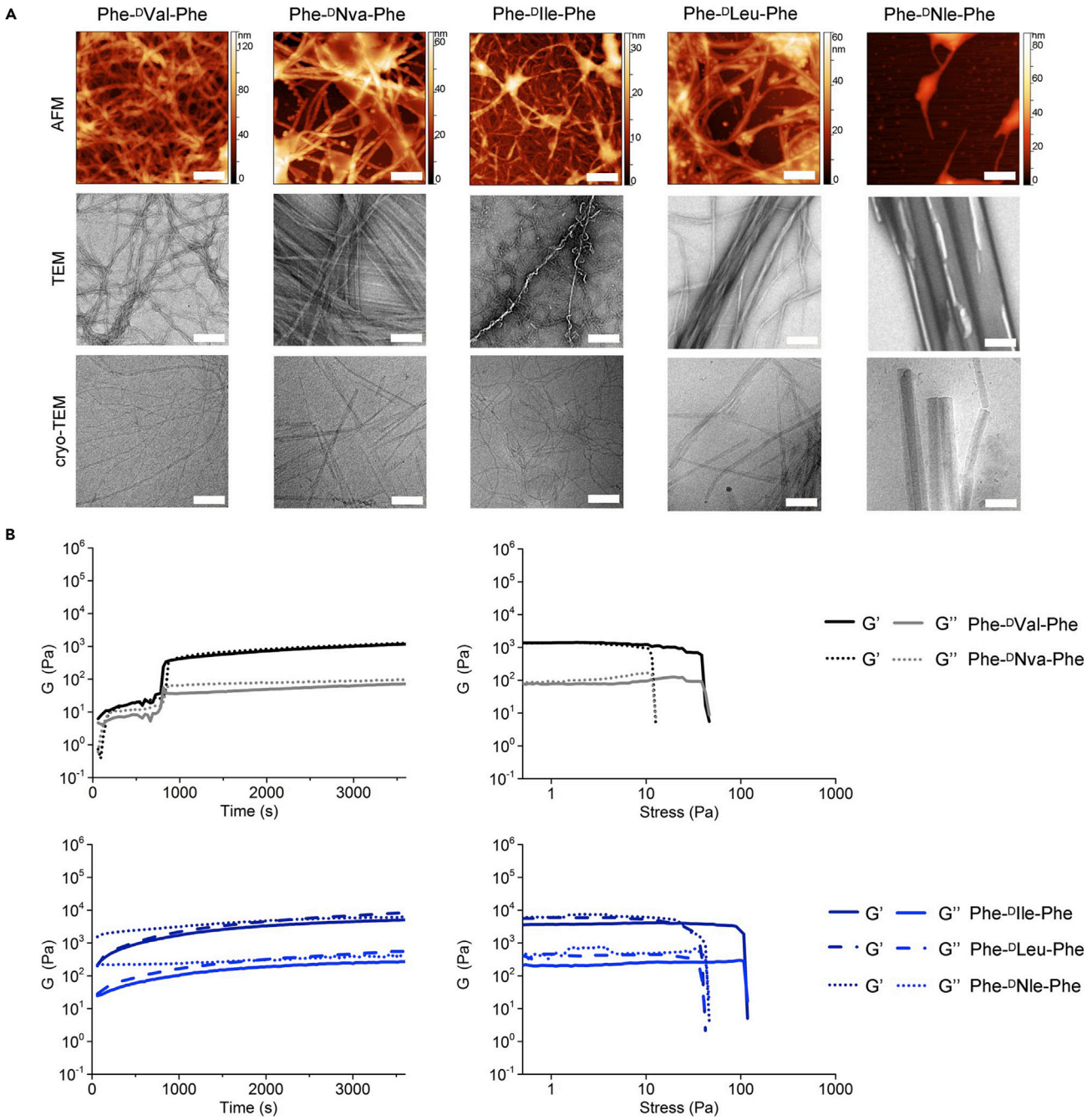

Figure 5. Nanostructured Hydrogel Morphology and Viscoelastic Properties

(A) AFM, TEM, and cryo-TEM images of the peptide hydrogels. Scale bars: 500 nm for AFM images (top row) and 200 nm for TEM and cryo-TEM images (central and bottom rows, respectively).

(B) Time sweep (left) and stress sweep (right) oscillatory rheometry measurements assessed the gel nature and the viscoelastic properties of peptide hydrogels containing a central amino acid with three (top) or four (bottom) methylene units in the aliphatic side chain.

Hydrogel Biomaterial Performance

All heterochiral peptides were tested for their cytotoxicity in fibroblast cell culture *in vitro*, in solution, or in the hydrogel state. Cell viability in solution was assessed with increasing concentrations up to the peptide solubility limit (2 mg mL^{-1} in 1% DMSO). Relative to that of the control, cell viability was greater than 90%, except

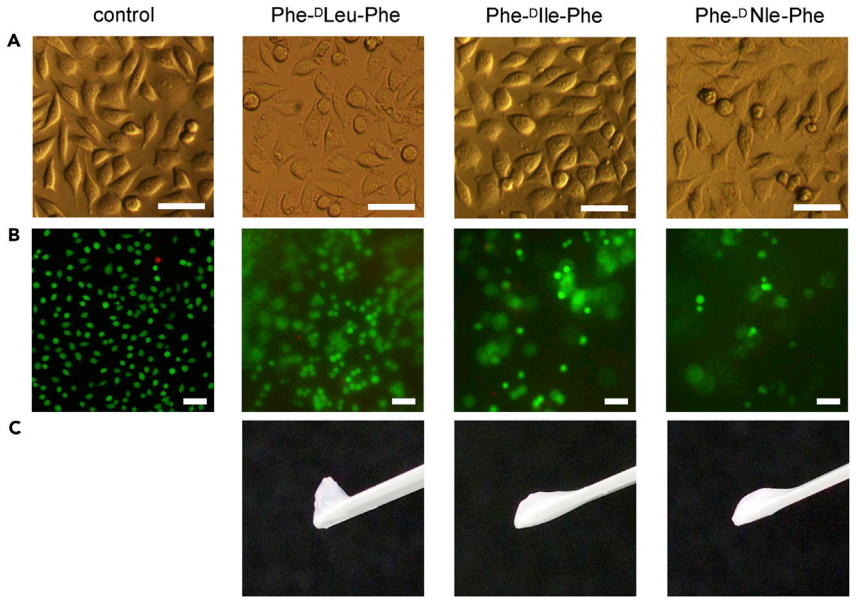

Figure 6. Peptide Performance under Fibroblast Cell-Culture Conditions

(A) Bright-field microscopy images of a cytotoxicity assay for peptides in solution at 2 mg mL^{-1} reveal spindle-morphology for spreading cells across all samples.

(B) Live (green) and dead (red) cell staining after 72 hr culture on peptide hydrogels reveals high cell viability and high cell numbers especially in the case of the Phe-^{D}Leu-Phe hydrogel.

(C) Photographs of peptide hydrogel samples after 72 hr under cell-culture conditions.

Scale bars: 50 μm.

that the two peptides bearing both a non-natural stereoconfiguration and a non-natural, linear side chain (i.e., ^{D}Nva and ^{D}Nle) led to cell viability in the range of 80%–90%, significantly lower than that of the control (see Figure S70). Cell morphology did not appear altered by the presence of peptides (Figures 6A and S71), except for the case of ^{D}Nle, where the number of round cells was significantly higher than the control; visible peptide fibrilization occurred over 24 hr at the highest concentration tested (Figure S71). Rare instances of rigid fibrils were noted also for the sample bearing ^{D}Nva, suggesting once again that the linear side chain favors peptide packing and fibrilization.

Peptide hydrogel stability against protease degradation was assayed *in vitro*. All heterochiral peptides resisted hydrolysis (<20% over 5 days), whereas non-assembling L-peptide analogs were completely digested within the first 24 hr (Figure S72). In addition, higher peptide hydrophobicity corresponded to slower gel dissolution, such that peptides bearing leucine isomers outperformed the others (Table S5) and were the only ones to persist after 72 hr in cell culture (Figures 6B and 6C). The Phe-^{D}Nle-Phe samples were not homogeneous, such that microscopic fiber bundles eventually segregated from the aqueous phase, in agreement with the observations discussed above. Nevertheless, the majority of cells were viable in all samples, and the greatest survival was observed in the Phe-^{D}Leu-Phe hydrogel. Overall, these results indicate that among peptides tested, Phe-^{D}Leu-Phe outperformed the others as a hydrogel biomaterial, and Phe-^{D}Nle-Phe consistently led to reduced cell spreading and viability in both solution and gel forms and was the peptide with the highest hydrophobicity and tendency toward fibrilization. We hypothesize that the combination of these factors with the presence of both a non-natural stereoconfiguration and a non-natural side chain resulted in significant, although limited, detrimental

effects in terms of biocompatibility and could be ascribed to the cells' limited ability to process this compound and its fibrils.

In conclusion, we present here a general design for hydrogel biomaterials from simple D- and L-amino acids in sets of three. Although the tripeptides are composed exclusively of hydrophobic amino acids, an amphiphilic conformation that is crucial to self-assembly emerges in the monomeric state. The characteristic monomer CD signature is correlated to kinked β strands according to Ramachandran plots, whereby only heterochiral—not homochiral—peptides succeed in segregating hydrophobic and hydrophilic zones to enable subsequent self-assembly in water. As a result, heterochiral tripeptide backbones bend in a turn to maximize non-covalent interactions and exclude water from specific regions, resulting in the superstructures zipping together. Tripeptide assembly is elucidated at each step by *in silico* and experimental data from the monomeric state and grows to fibrils, fibers, and macroscopic materials spanning from the angstrom scale to the nano-, micro-, and macroscales. The viscoelastic properties of the hydrogels are thus elucidated in terms of fiber diameter and interconnectivity, allowing correlation with amino acid side-chain length and branching. Finally, fibroblast viability data revealed no major toxicity and highlighted the potential use of the Phe-^{D}Leu-Phe hydrogel as a biomaterial. This investigation thus expands our understanding of how to use amino acid chirality in short peptides as a simple tool for designing and mastering complex supramolecular materials. Future work will extend this approach to other sequences featuring further functional groups and chirality combinations to provide a broader set of building blocks for functional supramolecular systems.

EXPERIMENTAL PROCEDURES

Peptide Preparation

Tripeptides were prepared according to standard Fmoc-based solid-phase peptide synthesis and purified on reverse-phase HPLC as previously described.[43] Spectroscopic and HPLC data are provided in Figures S3–S40 and Table S2.

Hydrogel Formation

Hydrogels were prepared by desolvation of each peptide in 0.1 M sodium phosphate (pH 11.8), after which an equal volume of 0.1 M sodium phosphate (pH 5.8) led to hydrogel formation at a final pH of 7.3 $\pm$ 0.1 within a few minutes. Peptide final concentrations used were 10 mM unless stated otherwise.

Molecular Modeling

Model structures of zwitterionic tripeptides Phe-Ala-Phe, Phe-^{D}Leu-Phe, and Phe-^{D}Ile-Phe were generated with MarvinSketch.[34] Structural analyses were performed with the AmberTools17 package[44] and through in-house *tcl* scripts run within the VMD1.9.3 software.[45]

All-Atom MD Simulations

Simulations were perfored with the AMBER16 simulation suite.[44]

Single Peptides

Each tripeptide was centered in a cubic box so that its distance from each face was at least 16 Å. The systems were solvated with ~2,500 water molecules. The parm14SB[46] and TIP3P[47] force fields were used for modeling peptides and water molecules. Structural relaxation was achieved in a multi-step fashion: first, a set of restrained optimization was performed up to 25,000 steps with the application of restraints (k = 1 kcal mol^{-1} Å^{-1}) to (1) all non-hydrogenous atoms of the system, (2)

backbone atoms, and (3) C_α atoms. The reference structures used for steps 2 and 3 were the final ones from the previous step. As the last step prior to MD, up to 50,000 cycles of unrestrained optimization were performed. Each system was then heated to 300 K in 1 ns via constant-pressure-temperature (NTP) MD simulations, followed by an equilibration phase of 10 ns. Starting from the equilibrated structure, an NTP MD simulation of 500 ns was performed for each system. Pressure and temperature were set to 1 atm and 300 K, respectively (after the equilibration phase), with the isotropic Berendsen barostat[48] and the Langevin thermostat,[49] respectively. A time step of 2 fs was used, and periodic boundary conditions were employed. Electrostatic interactions were evaluated with the Particle Mesh Ewald scheme with a cutoff of 9.0 Å for the short-range evaluation in direct space and for Lennard-Jones interactions (with a continuum model correction for energy and pressure).

Self-Assembly

MD simulations[35] were run for 216 tripeptides whose centers of mass were placed on a cubic 6 × 6 × 6 grid of 15-Å-spaced points. Initial orientations of peptides were randomized, and the system was solvated with ~40,000 water molecules. The initial volume of the box was ~1,203 $Å^3$, leading to a peptide concentration of ~0.2 M. Systems were equilibrated as described in the previous paragraph. Starting from the equilibrated structure, three independent NTP MD simulations, each 300 ns in length, were performed.

Theoretical CD Analysis

Theoretical CD spectra were calculated with the program DICHROCALC.[50] For each system, spectra were obtained as averages over 1,000 different conformations.

Microscopy

AFM,[43] cryo-TEM,[35] and TEM[35] images were acquired as previously described.

Cell-Culture Assays

Cytotoxicity in solution was assessed in accordance with ISO 10993; L929 mouse fibroblast cells were seeded at 10,000 cells per well of a 96-well tissue culture plate in 100 μL of medium (MEM + GlutaMAX [Gibco]) supplemented with 1 vol % nonessential amino acids (Gibco), 2 vol % antimycotic-antibiotic (Gibco), and 10 vol % fetal bovine serum (SAFC Biosciences) and were cultured overnight at 37°C and 5% CO_2. Peptides were dissolved in the medium with 1% DMSO at the highest concentration possible without the occurrence of precipitation or gelation, and 1:1 serial dilutions were prepared; peptide solutions were sterile filtered, and 100 μL was applied to monolayers that were then cultured further for 24 hr. Cells were imaged with an inverted microscope (Olympus IX71) before quantitation by reduction of resazurin (120 μL of a 1:9 solution of PrestoBlues in medium for 1.5 hr), and 100 μL was assayed for fluorescence on a Pherastar fluorometer (excitation 540/20 nm; emission 590/20 nm). Monolayers remained subconfluent throughout. For gel studies, gel precursor solutions were prepared as indicated previously, and 15 μL of each was mixed directly in triplicate wells of an uncoated μ-Slide for angiogenesis (Ibidi through DKSH). Gels with a lower peptide concentration were not tested to avoid premature gel dissolution during the assay. After 24 hr, gels were pretreated with 30 μL of medium for 1 hr. L929 cells were added to the gels (10,000 cells per cm^2 in 30 μL of medium) and cultured at 37°C in 5% CO_2 for up to 72 hr according to the manufacturer's instructions. Every 24 hr, cells had 30 μL of medium exchanged for fresh medium. Cell viability was investigated with the LIVE/DEAD assay (Invitrogen) according to the manufacturer's instructions. Cells were imaged with an inverted microscope (Nikon Eclipse TE2000-U) for calcein

(excitation 465–495 nm; emission 515–555 nm) and ethidium (excitation 510–560 nm; emission 4,590 nm).

Other experimental techniques are described in the Supplemental Information.

DATA AND SOFTWARE AVAILABILITY

Crystallographic data of L-Phe-Ala-Phe and Phe-DNva-Phe have been deposited in the Cambridge Crystallographic Data Center under accession numbers CCDC: 1588564 and 1836198, respectively.

ACKNOWLEDGMENTS

The authors gratefully acknowledge funding from the Italian Ministry of University and Research through the Scientific Independence of young Researchers program ("HOT-SPOT" project; personal research starting grant no. RBSI14A7PL to S.M.) and from the Ramón Areces Foundation (fellowship to A.M.G.). Single-crystal XRD data were acquired at the XRD1 line at Elettra Synchrotron in Trieste, Italy.

AUTHOR CONTRIBUTIONS

Investigation, A.M.G., D.I., E.P., K.E.S., L.J.W., C.D., M.M., and A.V.V.; Conceptualization, A.V.V. and S.M.; Writing, S.M. with contribution from all authors; Methodology, A.V.V., M.M., R.D.Z., and S.M.; Supervision, R.D.Z. and S.M.; Resources, M.G. and S.M.

DECLARATION OF INTERESTS

The authors declare no competing interests.

Accepted: May 24, 2018

REFERENCES AND NOTES

1. Draper, E.R., and Adams, D.J. (2017). Low-molecular-weight gels: the state of the art. Chem *3*, 390–410.

2. Cai, Y., Shen, H., Zhan, J., Lin, M., Dai, L., Ren, C., Shi, Y., Liu, J., Gao, J., and Yang, Z. (2017). Supramolecular "trojan horse" for nuclear delivery of dual anticancer drugs. J. Am. Chem. Soc. *139*, 2876–2879.

3. Alakpa, E.V., Jayawarna, V., Lampel, A., Burgess, K.V., West, C.C., Bakker, S.C.J., Roy, S., Javid, N., Fleming, S., Lamprou, D.A., et al. (2016). Tunable supramolecular hydrogels for selection of lineage-guiding metabolites in stem cell cultures. Chem *1*, 298–319.

4. Wang, H., Feng, Z., and Xu, B. (2017). Bioinspired assembly of small molecules in cell milieu. Chem. Soc. Rev. *46*, 2421–2436.

5. Zhou, J., Du, X., Berciu, C., He, H., Shi, J., Nicastro, D., and Xu, B. (2016). Enzyme-instructed self-assembly for spatiotemporal profiling of the activities of alkaline phosphatases on live cells. Chem *1*, 246–263.

6. Luo, Z., Wu, Q., Yang, C., Wang, H., He, T., Wang, Y., Wang, Z., Chen, H., Li, X., Gong, C., et al. (2017). A powerful $CD8^+$ T-cell stimulating D-tetra-peptide hydrogel as a very promising vaccine adjuvant. Adv. Mater. *29*, 1601776.

7. Scott, G.G., Mcknight, P.J., Tuttle, T., and Ulijn, R.V. (2016). Tripeptide emulsifiers. Adv. Mater. *28*, 1381–1386.

8. Lampel, A., Mcphee, S.A., Park, H.A., Scott, G.G., Humagain, S., Hekstra, D.R., Yoo, B., Frederix, P., Li, T.D., Abzalimov, R.R., et al. (2017). Polymeric peptide pigments with sequence-encoded properties. Science *356*, 1064–1068.

9. Zaramella, D., Scrimin, P., and Prins, L.J. (2012). Self-assembly of a catalytic multivalent peptide–nanoparticle complex. J. Am. Chem. Soc. *134*, 8396–8399.

10. Tao, K., Makam, P., Aizen, R., and Gazit, E. (2017). Self-assembling peptide semiconductors. Science *358*, https://doi.org/10.1126/science.aam9756.

11. Ung, P., and Winkler, D.A. (2011). Tripeptide motifs in biology: targets for peptidomimetic design. J. Med. Chem. *54*, 1111–1125.

12. Haubner, R., Gratias, R., Diefenbach, B., Goodman, S.L., Jonczyk, A., and Kessler, H. (1996). Structural and functional aspects of RGD-containing cyclic pentapeptides as highly potent and selective integrin $\alpha_v\beta_3$ antagonists. J. Am. Chem. Soc. *118*, 7461–7472.

13. Amiche, M., Delfour, A., and Nicolas, P. (1988). Structural requirements for dermorphin opioid receptor binding. Int. J. Pept. Protein Res. *32*, 28–34.

14. Henneberger, C., Papouin, T., Oliet, S.H.R., and Rusakov, D.A. (2010). Long-term potentiation depends on release of D-serine from astrocytes. Nature *463*, 232–236.

15. Kim, P.M., Duan, X., Huang, A.S., Liu, C.Y., Ming, G.L., Song, H., and Snyder, S.H. (2010). Aspartate racemase, generating neuronal D-aspartate, regulates adult neurogenesis. Proc. Natl. Acad. Sci. USA. *107*, 3175–3179.

16. Mahalakshmi, R., and Balaram, P. (2006). The use of D-amino acids in peptide design. In D-Amino Acids, R. Konno, H. Bruckner, A. D'Aniello, and G.H. Fisher, eds. (Nova Science Publishers, Inc.), pp. 415–428.

17. Gupta, J.K., Adams, D.J., and Berry, N.G. (2016). Will it gel? Successful computational prediction of peptide gelators using physicochemical properties and molecular fingerprints. Chem. Sci. *7*, 4713–4719.

18. Truong, W.T., Su, Y., Gloria, D., Braet, F., and Thordarson, P. (2015). Dissolution and degradation of fmoc-diphenylalanine self-assembled gels results in necrosis at high concentrations *in vitro*. Biomater. Sci. *3*, 298–307.

19. Wojciechowski, J.P., Martin, A.D., Mason, A.F., Fife, C.M., Sagnella, S.M., Kavallaris, M., and Thordarson, P. (2017). Choice of capping group in tripeptide hydrogels influences viability in the three-dimensional cell culture of tumor spheroids. Chempluschem *82*, 383–389.

20. Frederix, P.W., Scott, G.G., Abul-Haija, Y.M., Kalafatovic, D., Pappas, C.G., Javid, N., Hunt, N.T., Ulijn, R.V., and Tuttle, T. (2015). Exploring the sequence space for (tri-)peptide self-assembly to design and discover new hydrogels. Nat. Chem. *7*, 30–37.

21. Pappas, C.G., Shafi, R., Sasselli, I.R., Siccardi, H., Wang, T., Narang, V., Abzalimov, R., Wijerathne, N., and Ulijn, R.V. (2016). Dynamic peptide libraries for the discovery of supramolecular nanomaterials. Nat. Nanotechnol. *11*, 960–967.

22. Zhou, J., Li, J., Du, X., and Xu, B. (2017). Supramolecular biofunctional materials. Biomaterials *129*, 1–27.

23. Singh, V., Rai, R.K., Arora, A., Sinha, N., and Thakur, A.K. (2014). Therapeutic implication of L-phenylalanine aggregation mechanism and its modulation by D-phenylalanine in phenylketonuria. Sci. Rep. *4*, 3875.

24. Sievers, S.A., Karanicolas, J., Chang, H.W., Zhao, A., Jiang, L., Zirafi, O., Stevens, J.T., Münch, J., Baker, D., and Eisenberg, D. (2011). Structure-based design of non-natural amino-acid inhibitors of amyloid fibril formation. Nature *475*, 96–100.

25. Ridler, C. (2017). Alzheimer disease: misfolded diabetes-mellitus peptide seeds amyloid-beta aggregation. Nat. Rev. Neurol. *13*, https://doi.org/10.1038/nrneurol.2017.5.

26. Flemming, H.-C., Wingender, J., Szewzyk, U., Steinberg, P., Rice, S.A., and Kjelleberg, S. (2016). Biofilms: an emergent form of bacterial life. Nat. Rev. Micro. *14*, 563–575.

27. Banwell, E.F., Abelardo, E.S., Adams, D.J., Birchall, M.A., Corrigan, A., Donald, A.M., Kirkland, M., Serpell, L.C., Butler, M.F., and Woolfson, D.N. (2009). Rational design and application of responsive alpha-helical peptide hydrogels. Nat. Mater. *8*, 596–600.

28. Zhang, S. (2003). Fabrication of novel biomaterials through molecular self-assembly. Nat. Biotechnol. *21*, 1171–1178.

29. Zarzhitsky, S., Vinod, T.P., Jelinek, R., and Rapaport, H. (2015). Stacking interactions by two phe side chains stabilize and orient assemblies of even the minimal amphiphilic beta-sheet motif. Chem. Commun. (Camb.) *51*, 3154–3157.

30. Marchesan, S., Styan, K.E., Easton, C.D., Waddington, L., and Vargiu, A.V. (2015). Higher and lower supramolecular orders for the design of self-assembled heterochiral tripeptide hydrogel biomaterials. J. Mater. Chem. B *3*, 8123–8132.

31. Marchesan, S., Easton, C.D., Styan, K., Waddington, L., Kushkaki, K., Goodall, L., Mclean, K., Forsythe, J.S., and Hartley, P.G. (2014). Chirality effects at each amino acid position on tripeptide self-assembly into hydrogel biomaterials. Nanoscale *6*, 5172–5180.

32. Marchesan, S., Waddington, L., Easton, C.D., Winkler, D.A., Goodall, L., Forsythe, J., and Hartley, P.G. (2012). Unzipping the role of chirality in nanoscale self-assembly of tripeptide hydrogels. Nanoscale *4*, 6752–6760.

33. Pappas, C.G., Frederix, P.W.J.M., Mutasa, T., Fleming, S., Abul-Haija, Y.M., Kelly, S.M., Gachagan, A., Kalafatovic, D., Trevino, J., Ulijn, R.V., et al. (2015). Alignment of nanostructured tripeptide gels by directional ultrasonication. Chem. Commun. (Camb.) *51*, 8465–8468.

34. ChemAxon (2014). Marvin 14.1.9 ChemAxon (http://www.chemaxon.com).

35. Vargiu, A.V., Iglesias, D., Styan, K.E., Waddington, L.J., Easton, C.D., and Marchesan, S. (2016). Design of a hydrophobic tripeptide that self-assembles into amphiphilic superstructures forming a hydrogel biomaterial. Chem. Commun. (Camb.) *52*, 5912–5915.

36. Amdursky, N., and Stevens, M.M. (2015). Circular dichroism of amino acids: Following the structural formation of phenylalanine. Chemphyschem *16*, 2768–2774.

37. He, L., Navarro, A.E., Shi, Z., and Kallenbach, N.R. (2012). End effects influence short model peptide conformation. J. Am. Chem. Soc. *134*, 1571–1576.

38. Swindells, M.B., Macarthur, M.W., and Thornton, J.M. (1995). Intrinsic [ϕ],[ψ] propensities of amino acids, derived from the coil regions of known structures. Nat. Struct. Mol. Biol. *2*, 596–603.

39. Maynard, S.J., Almeida, A.M., Yoshimi, Y., and Gellman, S.H. (2014). New charge-bearing amino acid residues that promote beta-sheet secondary structure. J. Am. Chem. Soc. *136*, 16683–16688.

40. Ramachandran, G.N., Ramakrishnan, C., and Sasisekharan, V. (1963). Stereochemistry of polypeptide chain configurations. J. Mol. Biol. *7*, 95–99.

41. De Brevern, A.G. (2016). Extension of the classical classification of beta-turns. Sci. Rep. *6*, 33191.

42. Richardson, J.S. (1981). The anatomy and taxonomy of protein structure. Adv. Protein Chem. *34*, 167–339.

43. Garcia, A.M., Kurbasic, M., Kralj, S., Melchionna, M., and Marchesan, S. (2017). A biocatalytic and thermoreversible hydrogel from a histidine-containing tripeptide. Chem. Commun. (Camb.) *53*, 8110–8113.

44. Case, D.A., Cerutti, D.S., Cheatham, T.E., III, Darden, T.A., Duke, R.E., Giese, T.J., Gohlke, H., Goetz, A.W., Greene, D., Homeyer, N., et al. (2017). AMBER 2017 (University of California, San Francisco).

45. Humphrey, W., Dalke, A., and Schulten, K. (1996). VMD—visual molecular dynamics. J. Mol. Graph. *14*, 33–38.

46. Maier, J.A., Martinez, C., Kasavajhala, K., Wickstrom, L., Hauser, K.E., and Simmerling, C. (2015). Ff14SB: improving the accuracy of protein side chain and backbone parameters from ff99SB. J. Chem. Theory Comput. *11*, 3696–3713.

47. Jorgensen, W.L., Chandrasekhar, J., Madura, J.D., Impey, R.W., and Klein, M.L. (1983). Comparison of simple potential functions for simulating liquid water. J. Chem. Phys. *79*, 926–935.

48. Berendsen, H.J.C., Postma, J.P.M., Van Gunsteren, W.F., Dinola, A., and Haak, J.R. (1984). Molecular-dynamics with coupling to an external bath. J. Chem. Phys. *81*, 3684–3690.

49. Feller, S.E., Zhang, Y., Pastor, R.W., and Brooks, B.R. (1995). Constant pressure molecular dynamics simulation: The Langevin piston method. Time *103*, 4613–4621.

50. Bulheller, B.M., Rodger, A., and Hirst, J.D. (2007). Circular and linear dichroism of proteins. Phys. Chem. Chem. Phys. *9*, 2020–2035.